Original Article

Effect of boron addition on the hot ductility of SAE 5160 steel

Cynthia Serra Batista Castro [1]
André Luiz Assunção [2*]
Túlio César Nogueira [3]
Ermani Vinícius de Oliveira Lima [4]

Abstract

The effect of boron on the hot ductility of SAE 5160 steel was evaluated through computational simulations (Thermo-Calc® and DICTRA) and physical simulations carried out on a Gleeble® 3800 process simulator. Hot ductility tests were performed at heating rates of 10 °C/s, followed by cooling at two controlled rates (0.5 °C/s and 1 °C/s) to test temperatures between 700 °C and 1200 °C, which corresponds to the range in which billet straightening occurs. For each condition, the reduction of area was measured, and fracture surfaces were examined by SEM to identify the underlying fracture mechanisms. The results showed that boron addition significantly increases the hot ductility temperature range. For the higher cooling rate (1 °C/s), the boron-containing steel maintained reduction of area values above 70% across nearly the entire test interval, reaching approximately 90% at peak ductility, and eliminating the high-temperature embrittlement trough observed in the boron-free steel. These findings demonstrate that boron addition is beneficial to the hot ductility of SAE 5160 steel, provided that appropriate processing conditions are applied.

Keywords: Boron steel; Segregation; Hot ductility tests.

1 Introduction

The addition of boron to steel, even in small quantities, is known to improve its hardenability, resulting in greater mechanical strength and reduced costs with the addition of other alloying elements [1-3]. Furthermore, the presence of boron affects the macro and micro segregation of the elements that make up steel, leading to a higher concentration of these elements in the center of the billet, especially carbon [1]. This can cause a difference in hardenability across the thickness of the components and the presence of a greater number of inclusions in this region, increasing the possibility of cracking.

Many special steels are used in the automotive industry in applications that are subjected to cyclic movements, requiring high fatigue resistance. Any defect in the raw material, such as inclusions and cracks, can reduce fatigue resistance and eventually lead to material fracture. Therefore, it is necessary to seek adjustments to make the continuous casting process more reliable, minimizing or even eliminating the incidence of cracks.

Although boron improves hardenability, adding this element to steels can be detrimental to the continuous casting process, as these steels are more susceptible to cracking during continuous casting [1,4]. Studies have indicated that for steel with 0.001% boron by weight, there is a brittleness temperature range from 900 to 1300 °C [5,6].

The study of the influence of continuous casting parameters on hot ductility, such as chemical composition, temperature, cooling rates, and deformation, is important in terms of optimizing the continuous casting process, as mentioned by some authors [7-9].

To determine the optimal processing parameters, it is necessary to understand the ductile behavior of these materials within the temperature range between 700 °C and 1300 °C, which also includes the typical interval in which billet straightening occurs during continuous casting. It is equally important to evaluate the effect of adding alloying elements, such as boron, on the hot ductility of steels. For this purpose, hot ductility tests with in-situ melting were performed, enabling the analysis of the effects of cooling rates and deformation rates characteristic of the continuous casting process. Accordingly, this study aims to develop an integrated understanding of the effect of boron addition on the hot ductility of SAE 5160 steel, establishing the correlation between macro and microsegregation, precipitation phenomena, and the mechanical behavior across the critical temperature range of continuous casting.

[1]*Centro de Inovação e Tecnologia, Instituto SENAI de Inovação em Metalurgia e Ligas Especiais, Belo Horizonte, MG, Brasil.*
[2]*Gerência de Desenvolvimento de Produtos Indústria, ArcelorMittal, Belo Horizonte, MG, Brasil.*
[3]*Gerência de Qualidade, ArcelorMittal, Sabará, MG, Brasil.*
[4]*Gerência Técnica, ArcelorMittal, João Monlevade, MG, Brasil.*

**Corresponding author:* andre.assuncao@arcelormittal.com.br
E-mails: cscastro@fiemg.com.br, nogueira@arcelormittal.com.br, ermani.vo.lima@arcelormittal.com.br

2 Materials and methods

Table 1 shows the chemical compositions of the two steels used in this study, SAE 5160 (without boron) and SAE 51B60 (with boron), obtained by optical emission spectrometry, including the boron content. The steel sample, collected in the form of a double thickness "lollipop" specimen with a flat circular area of approximately 80 mm^2, was ground and polished to obtain a clean and homogeneous surface. The prepared sample was then analyzed using an ARL 4460 Optical Emission Spectrometer, which measures the characteristic emission lines of each element to quantify their concentrations.

Computational thermodynamic simulations were performed using Thermo-Calc® software to evaluate the effect of boron on the microsegregation of SAE 51B60 steel, using SAE 5160 steel as a reference.

The calculations were carried out using the TCFE9 thermodynamic and MOBFE4 kinetic databases. Since thermodynamic equilibrium calculations do not predict the redistribution of solutes during solidification, the solidification kinetics of SAE 51B60 steel were simulated.

Analyses of inclusions were performed using scanning electron microscopy (SEM) on SAE 5160 and SAE 51B60 steel billets in the regions indicated in Figure 1. As indicated in the figure, the region of the billet vertex will be referred to as the surface.

The analyses were performed on the cross section to the casting direction. The samples were embedded, sanded, and polished to 1 µm and analyzed without etching. The analyzed area was 2 x 2 mm^2, and Aztec/Steel (Oxford) software was used to classify the inclusions. This software has a particle analysis function (Feature) that allows the information of each particle (size, area, length, among others) and its chemical composition to be recorded.

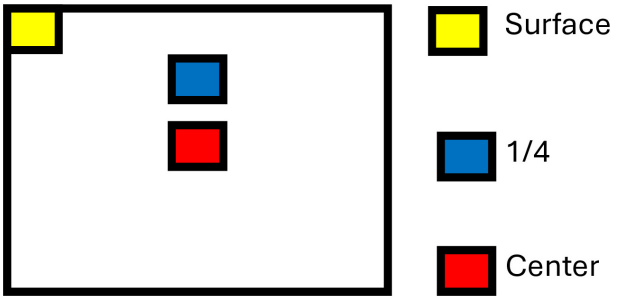

Figure 1. Schematic drawing of the cross section of the billet, indicating the regions where the samples were taken.

The Silicon Drift Detector (SDD) provides sensitivity to light elements, starting with boron (Z = 5). Elements such as boron, carbon, nitrogen, and oxygen can be detected, although with certain limitations related to signal intensity and peak resolution. For low-Z elements, inconsistencies may occur due to absorption of low-energy X-rays by the carbon coating or due to sample geometry, both of which can attenuate the detected signal. In addition, spectral peak overlaps (e.g., B Kα and C Kα) may introduce uncertainties in elemental identification. The detection efficiency for light elements is strongly affected by sample preparation, coating thickness, and the presence of surface contaminants. Moreover, the use of thin detector windows improves the transmission of low-energy X-rays, thereby enhancing sensitivity to elements such as boron, carbon, and nitrogen.

Hot ductility tests were performed on a Gleeble® 3800 process simulator, under vacuum, to evaluate the effect of boron on the hot ductility of SAE 5160 steel. For these tests, a single test specimen with a gauge length of 116.5 mm and a diameter of 10.0 mm in the longitudinal casting direction, was used for each experiment and heated at a rate of 10 °C/s to a temperature below the liquidus of the alloys, which was determined by computational thermodynamic simulation. They were held at these temperatures for 1 min to homogenize the microstructure and dissolve any precipitates present, and then cooled at two cooling rates, 0.5 °C/s and 1 °C/s, to test temperatures in the range of 700 °C to 1200 °C, values defined by simulation based on measurements obtained from the industrial process. Upon reaching the test temperature, the test specimen was kept at this T for homogenization and then tensioned to rupture at a strain rate of 6.0 x 10^{-4} s^{-1}.

Figure 2 shows the thermomechanical cycles for testing SAE 51B60 and SAE 5160 steels, respectively.

After the tests, the reduction of area was determined for each sample to evaluate the hot ductility of the test specimens from both steels. The reduction of area was calculated using the Equation 1:

$$RA = \frac{A_0 - A_f}{A_0} * 100 \quad (1)$$

where:
RA = reduction of area (%)
A_0 = initial cross-sectional area(mm^2)
A_f = final area at the fracture region (mm^2)

The fracture surfaces of the specimens of the two steels, obtained from the simulation tests on the Gleeble®, were analyzed by SEM to identify the fracture mechanisms present in each specimen.

Table 1. Chemical composition (% by mass) of SAE5160 and SAE51B60 steels.

Identification	C	Mn	Si	Cr	Al	B	Ti	S	P	N
AISI 51B60	0.58	0.86	0.27	0.83	0.020	0.0019	0.020	0.009	0.012	0,0025
AISI 5160	0.57	0.80	0.27	0.73	0.020	0.0004	0.003	0.009	0.010	0.0027

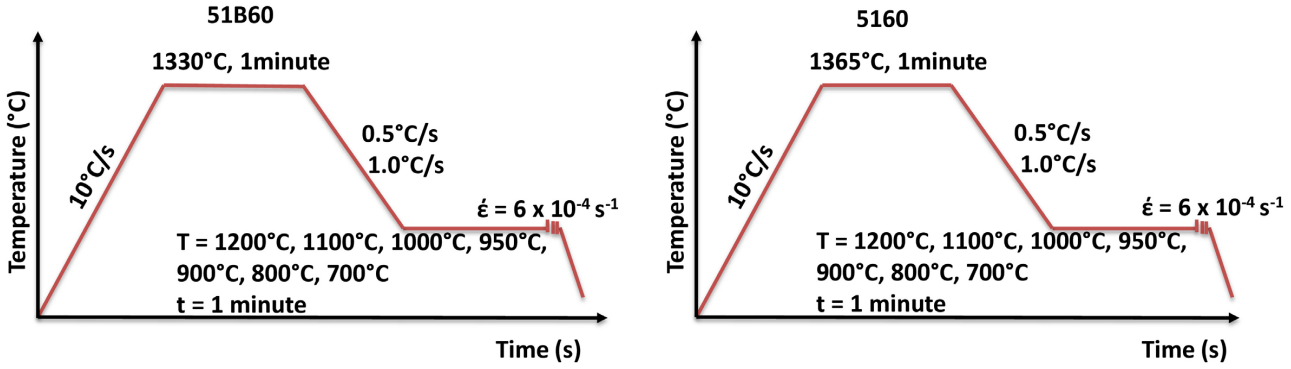

Figure 2. Thermomechanical cycles for SAE 51B60 and SAE 5160 steels.

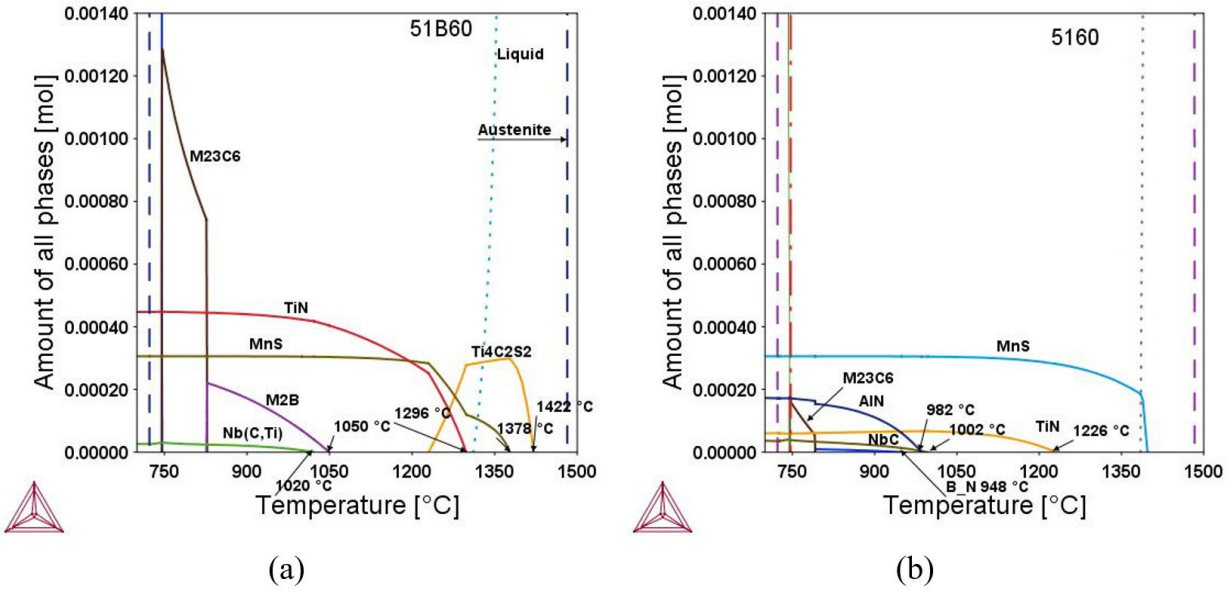

Figure 3. Thermodynamic simulation of SAE 51B60 (a) and SAE 5160 (b) steels.

3 Results and discussion

The results obtained from the simulations using Thermo-Calc® and Dictra are shown in Figures 3 and 4, respectively.

The plot showing the volume fraction of phases against temperature, Figure 3a, shows the precipitation of $Ti_4C_2S_2$ at 1422 °C, MnS at 1378 °C, both in the liquid, and TiN at 1296 °C, close to the liquid. It is also possible to observe a significant fraction of boron-rich M_2B at 1050 °C. An evaluation of the fraction of phases at 950 °C in this steel (SAE 51B60) shows a significant difference in the fraction of TiN, which is about 7 times higher compared to boron-free steel, Figure 3b. This result was expected since, as can be seen in Table 1, titanium in SAE 51B60 steel is higher, limiting the availability of nitrogen in solid solution, causing boron to remain free. It is known that coarse titanium carbonitrides formed in the liquid can have a negative effect on the toughness of the material. The location of titanium carbonitride precipitation in the billet depends on

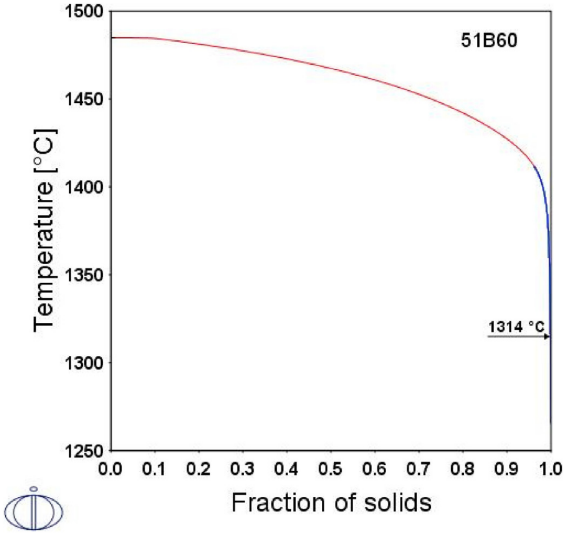

Figure 4. Solidification path of 51B60 steel simulated in DICTRA software showing temperature as a function of solid fraction. Red line: liquid + austenite; blue line: liquid + austenite + $Ti_4C_2S_2$ + MnS.

the titanium content and the processing conditions during continuous casting. It is expected that the amount of titanium carbonitride precipitates will be higher at the surface, since this is the first region to solidify. Titanium precipitates tend to form in greater numbers and with smaller sizes due to the reduced time available for growth. As solidification progresses, the residual liquid, enriched in solutes because of segregation ahead of the solid–liquid interface, becomes trapped between the dendrites. This condition makes the kinetics favorable for the nucleation and coarsening of precipitates in the central region of the ingot, which is the last region to solidify.

In addition, boron-rich precipitates, M_2B and B_N, are predicted by simulation in SAE 51B60 and SAE 5160 steels, respectively. In the latter, the amount of the B_N phase is small, and it may not form under industrial conditions.

Additionally, boron exerts relevant metallurgical effects during both solidification and the subsequent austenitic behavior. Small amounts of boron tend to segregate to grain boundaries, reducing their interfacial energy and stabilizing them, which slows boundary migration during reheating and promotes austenitic structures that are less prone to abnormal grain growth. Simultaneously, boron shows a strong tendency for interdendritic segregation, enriching the remaining liquid in the final stages of solidification and intensifying local microsegregation. This enrichment facilitates the early formation of boron-rich precipitates such as M_2B or B_N at high temperatures, resulting in particles that can grow significantly due to favorable kinetic conditions. Consequently, part of these precipitates is not fully dissolved during reheating, contributing to a heterogeneous distribution of particles in the matrix, a factor directly associated with lower microstructural refinement efficiency and increased susceptibility to abnormal grain growth, particularly in SAE 51B60 steel.

The result of the simulation in DICTRA, Figure 4, showed the solidification path of SAE 51B60 steel, completing solidification at around 1314 °C. This result, similar to that obtained by thermodynamic simulation, Figure 3a, is a relevant indication for greater enrichment of solutes in the interdendritic liquid, leading to greater microsegregation in solidification. A direct consequence is the promotion of nucleation of precipitates in the liquid at high temperatures enriched in microalloying elements. These precipitates have favorable kinetic conditions for coarsening and are not completely dissolved in the steel reheating stage, presenting a heterogeneous distribution in the matrix. This heterogeneity is one of the main factors responsible for the lower microstructural refinement, contributing to abnormal grain growth [10].

Considering the similarity between the results obtained by the simulations in DICTRA (Figure 4) and Thermo-Calc® (Figure 3a) for the end of solidification temperature of SAE 51B60 steel (1314 °C), the end of solidification temperature obtained via simulation by Thermo-Calc® (Figure 3b), 1358 °C, was considered for SAE 5160 steel.

Figure 5 shows the results of the inclusion analysis performed on the billet sample of SAE 5160 and SAE 51B60 steels in the surface, ¼, and center regions and Table 2 presents the inclusion density measured in each region for both steels. The data indicates that SAE 51B60 steel exhibits a considerably higher inclusion density across all regions, particularly at the surface, where the values are more than three times those observed for SAE 5160 steel. The same trend persists in the ¼ and center positions, where the differences between the steels also remain significant.

Although SAE 5160 and SAE 51B60 steels have practically the same Mn and S contents, boron steel has a higher MnS content (Figure 5). With practically the same S content available for both steels, this higher amount of MnS observed in SAE 51B60 steel can be associated with its lower solidus temperature (1314 °C) compared to SAE 5160 steel. In SAE 51B60 steel, MnS begins to precipitate at a temperature of 1378 °C (64 °C above the solidus temperature), while in SAE 5160 precipitation occurs only 12 °C above the solidus temperature. This greater temperature window of boron steel contributes to the enrichment of Mn in the segregated liquid at the solidification front, favoring MnS nucleation, indicating greater microsegregation in SAE 51B60 steel. As a result, faster cooling of SAE 51B60 steel reduces segregation in this steel, thus reducing the formation of coarse titanium carbonitrides and MnS.

Consequently, the higher inclusion densities reported in Table 2 reflect not only the precipitation kinetics of MnS but also the stronger segregation phenomena inherent to SAE 51B60 steel. As previously discussed, applying faster cooling conditions to this steel reduces the extent of segregation, thereby decreasing the formation of coarse titanium carbonitrides and MnS inclusions. Thus, the combined analysis of Figure 5 and Table 2 reinforces the metallurgical mechanisms governing inclusion formation and highlights the effects of boron on solidification behavior and microsegregation patterns.

Figure 6 shows comparisons of the hot ductility curves for SAE 5160 and SAE 51B60 steels considering cooling rates of 0.5 (Figure 6a) and 1 °C/s (Figure 6b). The dashed line on the horizontal axis represents the critical area reduction value for embrittlement. According to the literature [11], this value can vary from 40 to 60% depending on the appearance of the fractures presented by the material. The value of 60%, as indicated in the figures, was determined based on the results of fractographic analyses that were obtained and will be presented later. Above this value of 60%, the material exhibits satisfactory ductile behavior, and below this value, it exhibits ductile behavior, but insufficient.

Figure 6 shows that SAE 5160 steel exhibits similar qualitative behavior for both cooling rates, with the first embrittlement trough occurring at approximately 800 °C, although with different intensities. The second embrittlement trough appears at higher temperatures but in distinct ranges depending on the cooling rate. At intermediate temperatures, both rates display a marked increase in ductility, with RA

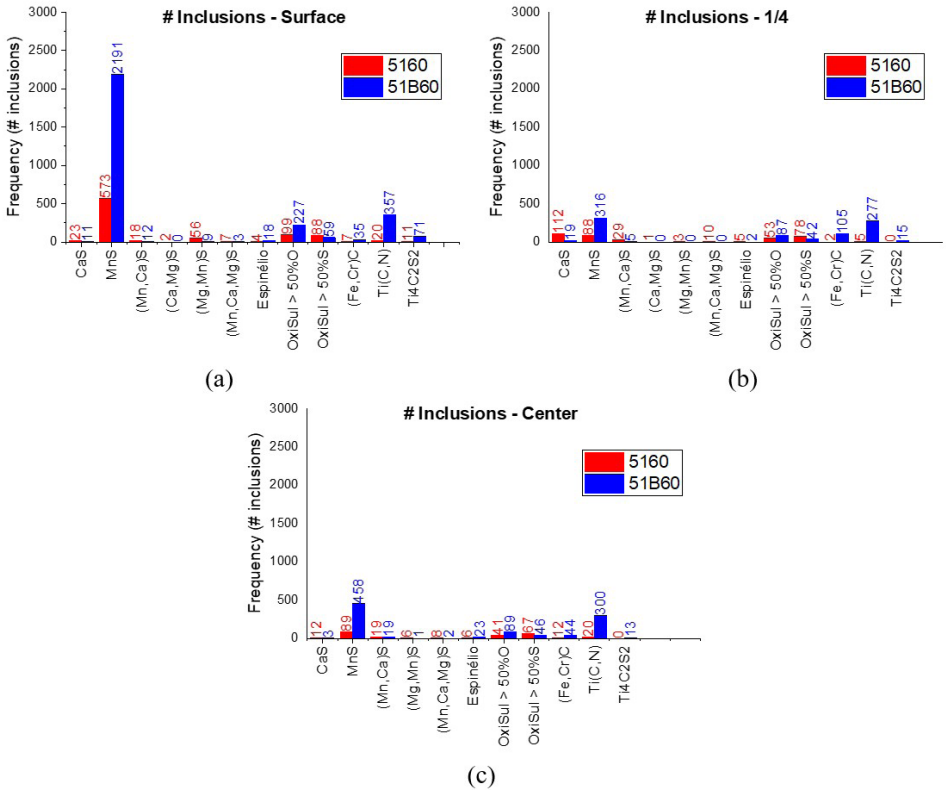

Figure 5. Comparison of the frequency of inclusions and particles between SAE5160 and SAE51B60 steels. (a) Billet surface (b) ¼ region of the billet (c) Center of the billet.

Table 2. Inclusion density of SAE 5160 and SAE 51B60 steels.

Steel	Region	Inclusion density
AISI 51B60	Surface	748
	1/4	217
	Center	250
AISI 5160	Surface	227
	1/4	97
	Center	70

reaching values close to 90% around 900 °C. For the 1 °C/s rate, this high ductility condition is also observed at 950 °C. For the 0.5 °C/s rate, the most favorable working range lies between 1100 °C and 1200 °C, where RA remains above 60%. At 1 °C/s, suitable working temperatures would be between 900 °C and 950 °C, provided such low temperatures are operationally viable, or at 1200 °C.

For SAE 51B60 steel, at 0.5 °C/s, ductility remains high (RA > 60%) between 700 °C and 950 °C, reaching approximately 90% in this interval. A significant reduction in RA occurs between 1000 °C and 1100 °C, reaching a minimum of 25% at 1000 °C, followed by recovery to nearly 90% at 1200 °C. At 1 °C/s, SAE 51B60 steel maintains consistently high ductility from 700 °C to 1100 °C, with the lowest RA value around 70% at 700 °C and no embrittlement pits within this temperature range. Only at 1200 °C is observed (minimum RA ≈ 50%), likely due to the presence of interdendritic liquid. These results reinforce the general observation that the higher the strain rate, the better the hot ductility of the steel [12]. Thus, for the boron-added steel, increasing the cooling rate substantially broadens the high-ductility temperature range. These trends are consistent with previous studies [11,13] and more recent investigations by Zheng et al. [12], who demonstrated that optimized Ti–B additions significantly improve hot ductility by reducing segregation induced grain boundary weakening when processing parameters are properly controlled.

Considering both steels, the comparison between Figures 6a and 6b shows that the 1 °C/s rate consistently yields broader and more stable high-ductility regions. At 0.5 °C/s, the ductile windows are narrower and the embrittlement troughs more pronounced (minimum RA ≈ 20%). At 1 °C/s, the minimum RA for SAE 5160 increases to roughly 40%, and SAE 51B60 remains highly ductile across almost the entire temperature range, showing no identifiable embrittlement troughs.

After the hot ductility tests on the Gleeble®, fractographic analyses by SEM were performed to correlate fracture mechanisms with the measured RA values. High RA values correspond to transgranular ductile fracture, whereas intergranular fracture is characteristic of low-ductility specimens. Mixed mode fractures contain both transgranular and intergranular features, each of which may display ductile or brittle aspects.

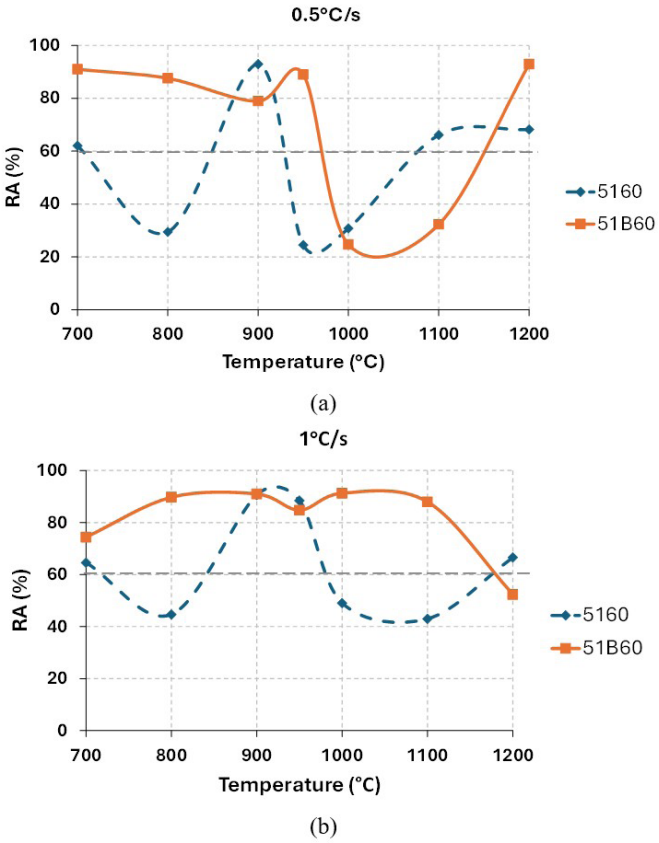

Figure 6. Comparison of hot ductility curves for SAE 5160 and SAE 51B60 steels for cooling rates of 0.5 °C/s (a) and 1 °C/s (b).

The fractographic and microstructural analyses provide a consistent explanation for these behaviors. The intergranular fracture observed in conditions where RA < 60% is closely linked to the presence of segregated MnS and, in the case of the boron steel, precipitates rich in boron such as B_2N. As shown in Figure 5, SAE 51B60 contains a higher density of MnS inclusions, resulting from its wider MnS precipitation window associated with a lower solidus temperature (1314 °C). This promotes significant Mn enrichment in the interdendritic liquid, forming continuous or semi-continuous MnS films along grain boundaries. These films reduce grain-boundary cohesion and act as preferential sites for cavity nucleation, accounting for the strong intergranular fracture found in regions of low RA.

It is commonly stated in the literature that a minimum RA value, typically 40% or 60%, is required to identify processing conditions that minimize crack formation during continuous casting. However, the determination of this critical ductility is largely empirical and depends strongly on the steel grade and testing conditions. Nagasaki et al. (1999), as cited by Chown [11], proposed RA as the criterion distinguishing transgranular ductile fracture from intergranular fracture, although the numerical threshold is highly dependent on test conditions.

In the present study, for all temperatures and cooling rates where RA values were below 60%, intergranular fracture was observed, as shown in Figure 7. The only exception occurred for the SAE 5160 steel specimens tested at 700 °C under cooling rates of 0.5 °C/s and 1 °C/s, which exhibited RA values of 62% and 65%, respectively, very close to the critical threshold. These specimens displayed mixed fracture modes, as expected for values lying within the RA transition region.

Fractographic analyses were performed on the fracture surfaces of all specimens to confirm their fracture characteristics. Figures 8 and 9 illustrate the fractured surfaces of specimens from SAE 5160 and SAE 51B60 steels that resulted in a high reduction of area of around 90% and less than 60%, respectively. In specimens with a reduction of area of around 90%, the high hot ductility of the material is related to ductile transgranular failures, the mechanism of which is the growth and coalescence of deep microcavities (dimples). For samples with a reduction of area of less than 60%, which constitute the embrittlement points in Figure 6, the embrittlement of steels is mainly characterized by the presence of intergranular fracture.

Figure 10 shows the surface of the sample with a reduction of area close to the critical value.

In this case, it is possible to observe from the surface characteristics that this is a mixed-character fracture, with the presence of deep dimples, indicating transgranular ductile fracture, the presence of intergranular brittle fracture, and honeycomb-shaped microcavities, characteristic of intergranular ductile fracture.

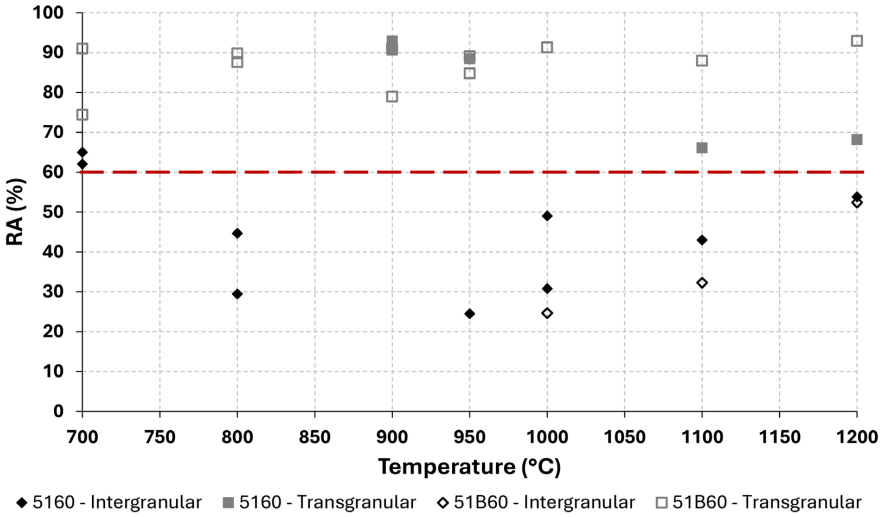

Figure 7. Area reduction dependence with the fracture mechanism for SAE 5160 and SAE 51B60 steels.

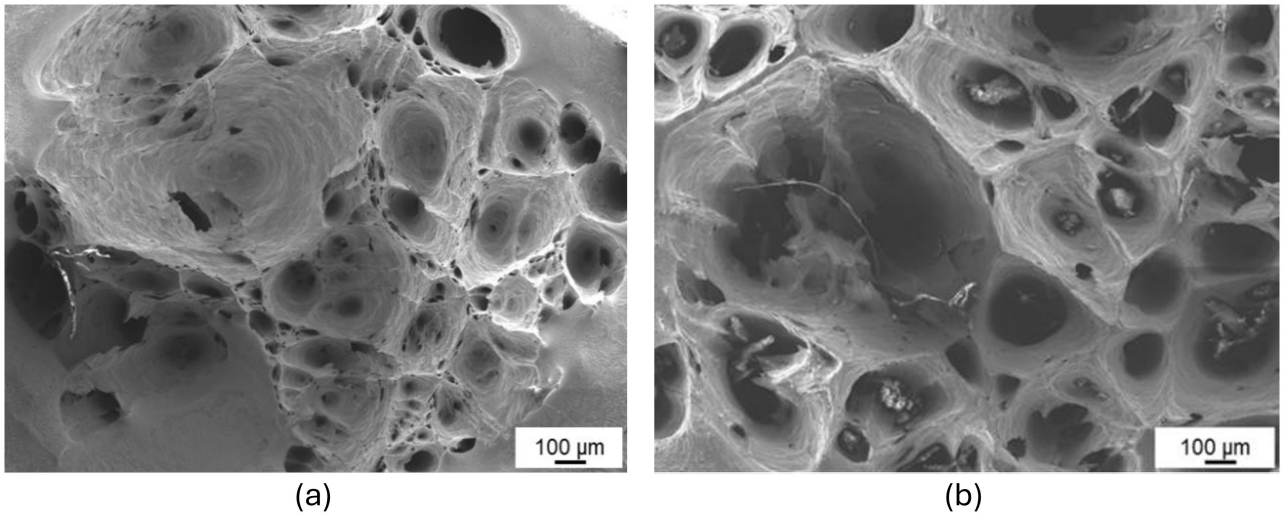

Figure 8. Fracture surface of the specimens tested at a cooling rate of 0.5 °C/s for the steels (a) SAE 5160 (T = 900 °C) and (b) SAE 51B60 (T = 950 °C).

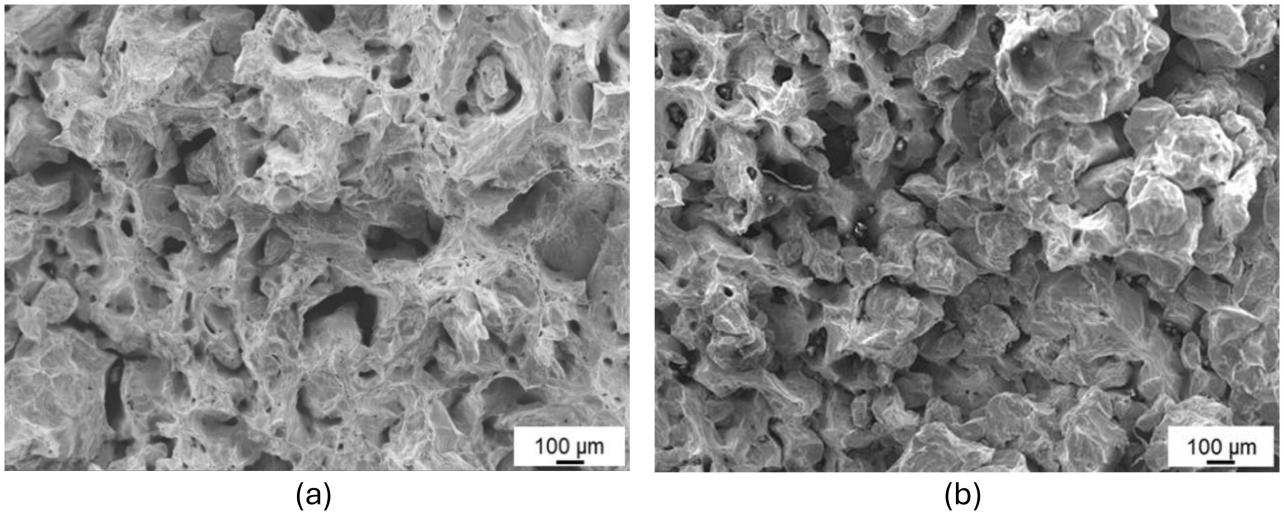

Figure 9. Fracture surface of the specimens tested at a cooling rate of 0.5 °C/s for the steels (a) SAE 5160 (T = 900 °C) and (b) SAE 51B60 (T = 950 °C).

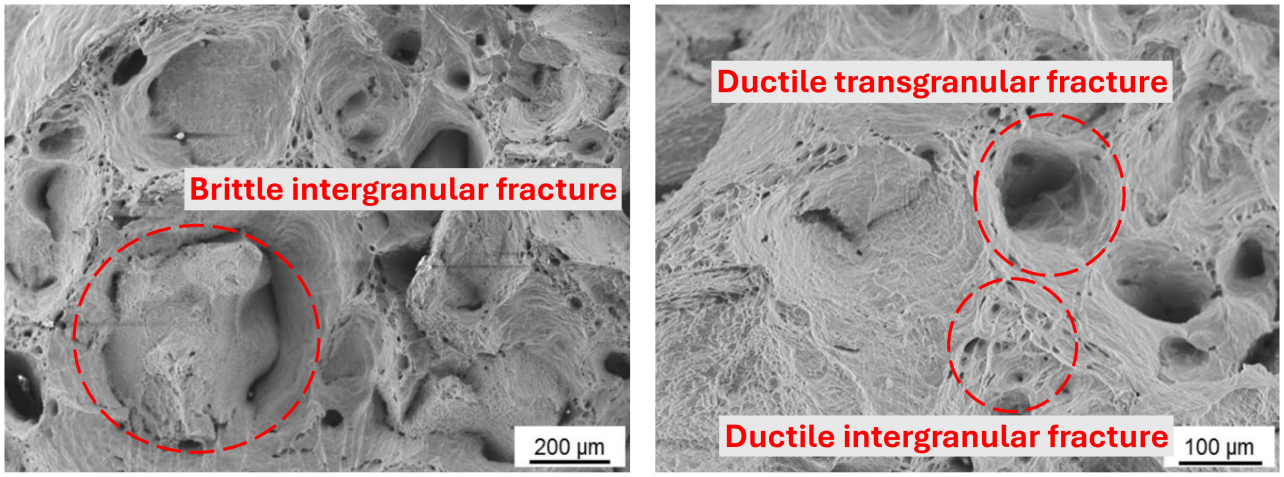

Figure 10. Fracture surface of SAE 5160 steel tested at a cooling rate of 0.5 °C/s at a temperature of 700 °C, (a) 75x and (b) 160x, showing characteristics of brittle and ductile intergranular fracture and ductile transgranular fracture, SEM.

4 Conclusions

The results showed that the boron-containing steel (SAE 51B60) exhibited a lower solidus temperature (1314 °C) compared to SAE 5160, which led to a wider solidification interval and consequently greater microsegregation. This condition favored the precipitation of MnS and boron-rich phases along interdendritic regions and grain boundaries, contributing to embrittlement under inadequate processing conditions.

The analyses also demonstrated that increasing the cooling rate mitigates these effects. In particular, the higher cooling rate of 1 °C/s significantly reduced segregation and the precipitation of coarse particles, resulting in consistently higher ductility across a broader temperature range. Under this condition, SAE 51B60 steel maintained reduction of area values above 70% in nearly the entire test interval, eliminating the embrittlement trough observed at lower cooling rates.

Based on the hot ductility behavior of both steels, the ideal processing window to minimize crack susceptibility during continuous casting corresponds to the range between 700 °C and 1100 °C, in which the reduction of area remains above 60% for both alloys when cooled at 1 °C/s. In the case of SAE 5160 steel, it is observed that at this cooling rate the material exhibits high ductility mainly between 900 and 950 °C, while still maintaining RA values above 60% throughout part of the intermediate temperature range up to approximately 1100 °C. These results confirm that the addition of boron is beneficial to hot ductility, if processing conditions, especially cooling rate and straightening temperature are properly controlled.

Acknowledgements

The authors would like to thank ArcelorMittal and the Institute for Innovation in Metallurgy and Special Alloys CIT SENAI for their support and infrastructure in the development of this R&D project.

References

1 Sun J, Zhua H, Wang W, Duan Y. Effect of boron segregation on the surface crack of low carbon boron-bearing steel. Results in Physics. 2019;13:102153. https://doi.org/10.1016/j.rinp.2019.02.089.

2 Deva A, Jha BK, Mishra NS. Influence of boron on strain hardening behaviour and ductility of low carbon hot rolled steel. Materials Science and Engineering A. 2011;528(24):7375-7380. https://doi.org/10.1016/j.msea.2011.06.030.

3 Wang XM, He XL. Effect of boron addition on structure and properties of low carbon bainitic steels. ISIJ International. 2002;42(Suppl):38-46. https://doi.org/10.2355/isijinternational.42.Suppl_S38.

4 Shen K, Wang SF, Ma H, Liao SL. Analysis and improving measures for surface defects on low carbon boron steel. Journal of Iron and Steel Research. 2014;26(1):57-62.

5 Kim SI, Choi SH, Lee Y. Influence of phosphorous and boron on dynamic recrystallization and microstructures of hot-rolled interstitial free steel. Materials Science and Engineering A. 2005;406(1):125-133. https://doi.org/10.1016/j.msea.2005.06.040.

6 He XL, Chu YY, Jonas JJ. Grain boundary segregation of boron during continuous cooling. Acta Metallurgica. 1989;37(1):147-161. https://doi.org/10.1016/0001-6160(89)90274-5.

7 Castilhos E, Janoski J, Fernandes PC, Strohaeecker T. Contribuição para a caracterização e diminuição da ocorrência de defeitos internos do tipo trinca off-corner em barras laminadas. In: Anais do 45º Seminário de Aciaria – Internacional; 2014; Porto Alegre; Brasil. São Paulo: ABM; 2014. p. 898-908.

8 Shi C-B, Liu W-J, Li J, Yu L. Effect of boron on the hot ductility of low-carbon Nb-Ti-microalloyed steel. Materials Transactions. 2016;57(5):647-653. https://doi.org/10.2320/matertrans.M2015388.

9 Carpenter KR, Dippenaar R, Killmore CR. Hot ductility of Nb- and Ti-bearing microalloyed steels and the influence of thermal history. Metallurgical and Materials Transactions. A, Physical Metallurgy and Materials Science. 2009;40A(3):573-580. https://doi.org/10.1007/s11661-008-9749-1.

10 Liu Y, Militzer M, Perez M. Phase field modelling of abnormal grain growth. Materials (Basel). 2019;12(24):1-20. https://doi.org/10.3390/ma12244048.

11 Chown LH. The influence of continuous casting parameters on hot tensile behavior in low carbon, niobium and boron steels [thesis]. Johannesburg: University of the Witwatersrand; 2008.

12 Zheng YM, Zhang L, Lin Y, Wang J, Wang K, Guo Z, et al. Effect of compound addition of Ti–B on hardenability and hot ductility of 22MnB5 hot stamped steel. Journal of Materials Research and Technology. 2025;36:1173-1193. https://doi.org/10.1016/j.jmrt.2025.03.189.

13 Zarandi F, Yue S. The effect of boron on hot ductility of Nb-microalloyed steels. ISIJ International. 2006;46(4):591-598. https://doi.org/10.2355/isijinternational.46.591.

Received: 7 Oct. 2025
Accepted: 25 Dec. 2025

Editor-in-charge:
André Luiz Vasconcellos da Costa e Silva